Optimal Control of Film Growth in Lithium-Ion Battery Packs via Relay Switches

Scott J. Moura, *Student Member, IEEE,* Joel C. Forman, Saeid Bashash, *Member, IEEE,*
Jeffrey L. Stein, Hosam K. Fathy

Abstract—Recent advances in lithium ion battery modeling suggest unequal but controlled and carefully timed charging of individual cells by reduce degradation. This article compares anode-side film formation for a standard equalization scheme versus unequal charging through switches controlled by deterministic dynamic programming (DDP) and DDP-inspired heuristic algorithms. A static map for film growth rate is derived from a first-principles battery model adopted from the electrochemical engineering literature. Using this map, we consider two cells connected in parallel via relay switches. The key results are: (1) Optimal unequal and delayed charging indeed reduces film buildup; (2) A near-optimal state feedback controller can be designed from the DDP solution and film growth rate convexity properties. Simulation results indicate the heuristic state-feedback controller achieves near optimal performance relative to the DDP solution, with significant reduction in film growth compared to charging both cells equally, for several film growth models. Moreover, the algorithms achieve similar film reduction values on the full electrochemical model. These results correlate with the convexity properties of the film growth map. Hence, this article demonstrates that unequal charging may indeed reduce film growth given certain convexity properties exist, lending promise to the concept for improving battery pack life.

Index Terms—Lithium-ion batteries, health management, battery management systems, optimal control, dynamic programming.

I. INTRODUCTION

THIS article examines the problem of optimizing charging for individual modules in a battery pack such that the pack's overall health degradation is minimized. Such health-conscious battery pack management has the potential to increase the useful life and reduce the long-term replacement costs of expensive high-capacity battery packs. This is important for ensuring the financial feasibility of battery energy storage in systems such as electric vehicles and smart grids, especially if such systems are able to share energy through, e.g.,

S. J. Moura, J. C. Forman, S. Bashash, and J. L. Stein are with the Department of Mechanical Engineering, University of Michigan, Ann Arbor, MI 48109-2133 USA (e-mail: sjmoura@umich.edu; jcforman@umich.edu; bashash@umich.edu; stein@umich.edu).

H. K. Fathy is with the Department of Mechanical and Nuclear Engineering, Pennsylvania State University, University Park, PA 16802 USA (Address all correspondences to this author; phone: +1-814-867-4442; e-mail: hkf2@psu.edu).

vehicle-to-grid (V2G) integration [1]. The article's overall goal is therefore to design battery pack management algorithms that control degradation in some optimal sense. We pursue this goal specifically for a pack consisting of two modules connected in parallel. Moreover, we specifically focus on lithium ion chemistries, which have been identified as a promising battery technology for achieving high energy and power densities, among other benefits [2]. Managing degradation is particularly challenging because the associated mechanisms, including resistive film growth at the anode, are typically simulated using computationally intensive electrochemistry-based models that may not be directly conducive to control design. Furthermore, it is currently impractical to directly access and control the mechanisms causing degradation inside the cell. To address these issues, we construct a simple map-based model of battery degradation and use it to design a nearly optimal controller that utilizes existing relays in high-energy capacity battery packs.

Previous research has examined at least three important problems related to health-conscious battery management. First, researchers have developed cell-to-cell charge equalization circuits that protect cells connected in series strings from over-charging or over-discharging due to capacity imbalances [3]–[6]. This article proposes an additional battery health management algorithm at the cell module level. Specifically, we consider the potential advantages of allowing *unequal* charge values across modules connected in parallel, and allow flexibility in determining the *timing* of the charge process.

Second, the literature on lithium ion batteries also addresses the problem of modeling battery degradation, power fade, and capacity fade. A popular model for capturing the lithium diffusion dynamics and intercalation phenomena was developed by Doyle, Fuller, and Newman in [7], [8]. This model is particularly appealing because it accurately captures the diffusion dynamics and voltage response characteristics relevant for a wide range of electrolyte materials and physical parameters. Ramadass *et al.* [9] extended this model to study capacity fade by hypothesizing an irreversible solvent reduction reaction at the anode-side electrode/electrolyte interface that generates a resistive film by consuming cyclable lithium. Because this process is considered one of the chief contributors to capacity fade and power loss [10]–[12], this article uses the model presented in [9] to study battery health management.

Finally, although there have been few publications on *controlling* battery health degradation, the concept of modeling battery degradation in terms of charge capacity fade and increased internal resistance spawned a body of research known as state-of-health (SOH) estimation. Research on SOH

estimation generally uses empirical equivalent circuit battery cell models to estimate charge capacity and internal resistance, using a variety of algorithms, such as batch data reconciliation, moving-horizon parameter estimation [13], recursive least squares [14], and extended Kalman filtering [15]–[17]. Recently, Smith, Rahn, and Wang [18] and Di Domenico, Fiengo, and Stefanopoulou [19] respectively used linear and extended Kalman filters to estimate the internal spatial-temporal states of reduced order electrochemical models derived from [7], [8]. This work does not estimate SOH-related parameters, however.

The main goal of this article is to extend the above research on battery health management by adding four important and original contributions. First, we utilize a high-fidelity electrochemistry-based model of film growth to generate a reduced degradation model more suitable for control design. Second, we set up a technique for active control of film growth that uses existing relay switches in battery packs, typically designed to prevent thermal runaway. Third, we formulate an optimal control problem that seeks to minimize total battery pack film growth through appropriate relay switching sequences. Fourth, we demonstrate that a nearly optimal control policy can be implemented as a set of heuristic rules, designed from the optimal control results and convexity properties of film growth rate. Portions of this work have been previously published in non-archival form [20]; however this article adds significant new material which validates the aforementioned controllers on a high-fidelity electrochemistry-based battery model and alternative cycles and film growth parameterizations. In summary, the aim of this article is to extend dynamic systems battery health research into the arena of lithium-ion film growth control. Namely, this article demonstrates that film growth can be reduced through novel charge unequalization schemes when certain convexity properties of the film growth map exist.

The remainder of the article is organized as follows: Section 2 reviews an electrochemical model for film growth developed by Ramadass, *et al.* [9], the reduced model utilized in this article, and a simple battery pack design. Section 3 formulates a deterministic dynamic programming (DDP) problem for minimizing total film growth in the battery pack under consideration. Section 4 analyzes the DDP results and interprets the solution via the convexity properties of film growth rate. We also consider the same optimization process for alternative film growth maps. This analysis motivates the design of a suboptimal heuristic feedback control law. Section 5 characterizes the performance of the heuristic algorithm vis-a-vis the DDP solution and standard charge equalization scheme, both on the equivalent circuit model used for optimization and the full electrochemical model. Finally, Section 6 summarizes the article's main conclusions.

II. MODEL DEVELOPMENT

A. Electrochemical Capacity Fade Mechanics

In this article, a function mapping cell state of charge (SOC) and current to film growth rate is extracted from a first-principles electrochemical Li-ion battery cell model adopted from [9]. This model simulates phenomena such as lithium
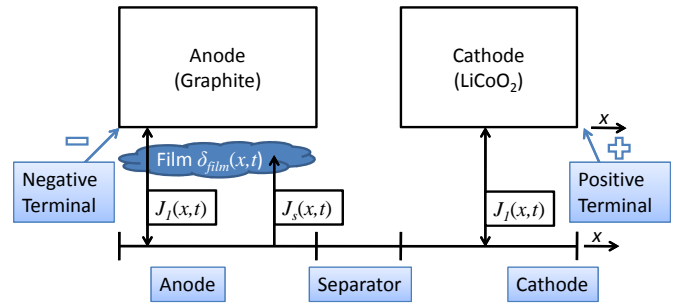

Fig. 1. Structure of the electrochemical lithium-ion battery cell model.

ion diffusion and intercalation to determine the potential and concentration gradients in the solid and solution sections of the anode, cathode, and separator. A schematic of the cell model is provided in Fig. 1, where Ramadass *et al.* argue that a resistive film builds up on the anode electrode/electrolyte interphase [9]. The exact chemical side reaction depends on the chemistry of the electrode and electrolyte. Equations (1)-(6), developed by Ramadass *et al.* argue that a simple and general method for modeling capacity loss is to assume an irreversible solvent reduction reaction of the following form

$$S + Li^+ + e^- \rightarrow P \tag{1}$$

where S denotes the solvent species and P is the product.

As a result of this irreversible side reaction, the products form a film at the electrode/electrolyte interface, which has a time and spatially varying thickness $\delta_{film}(x,t)$. This irreversibly formed film combines with the initial solid electrolyte interphase (SEI) resistance R_{SEI} to compose the total resistance at the electrode/electrolyte interface as follows

$$R_{film}(x,t) = R_{SEI} + \frac{\delta_{film}(x,t)}{\kappa_P} \tag{2}$$

where κ_P, denotes the conductivity of the film, x is the spatial coordinate, and t is time. The state equation corresponding to the growth of film thickness, due to the unwanted solvent reduction described in Eq. (1), is given by

$$\frac{\partial \delta_{film}(x,t)}{\partial t} = -\frac{M_P}{a_n \rho_P F} J_s(x,t) \tag{3}$$

In Eq. (3), M_P, a_n, ρ_P, and F represent the product's molecular weight, specific surface area, mass density, and Faraday's constant, respectively. The term J_s denotes the local volumetric current density for the side reaction, which is governed by Butler-Volmer kinetics. If we assume the solvent reduction reaction is irreversible and the variation of Li-ion concentration in the solution is small, then we may approximate J_s by the following Tafel equation [21].

$$J_s(x,t) = -i_{0,s} a_n e^{\left(\frac{-0.5F}{RT}\eta_s(x,t)\right)} \tag{4}$$

In Eq. (4), $i_{0,s}$, R, and T respectively denote the exchange current density for the side reaction, universal gas constant, and cell temperature. The term η_s represents the side reaction overpotential, which drives the solvent reduction reaction in Eq. (1). This variable is expressed by the following equation,
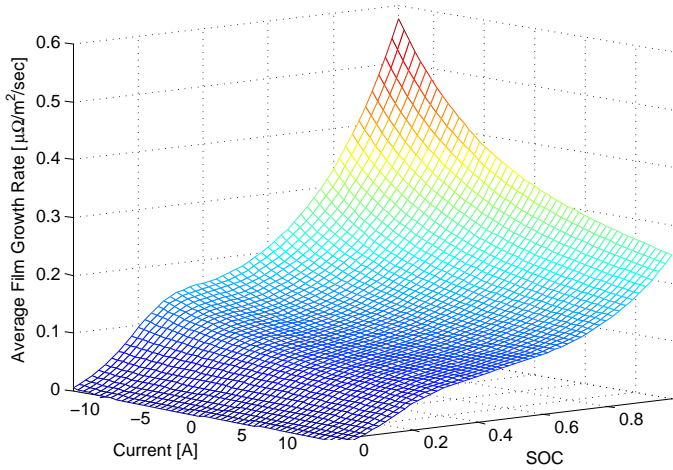
Fig. 2. Static approximation of film growth rate vs. cell current and SOC for fresh, relaxed cell (i.e. $\delta_{film} = 0$ and concentration distributions are constant). Positive current corresponds to discharge.

Fig. 3. Circuit diagram of battery pack.

based on Kirchoff's voltage law.

$$\eta_s(x,t) = \Delta\phi(x,t) - U_{s,ref} - \frac{J_{tot}(x,t)}{a_n} R_{film}(x,t) \quad (5)$$

The variable $\Delta\phi$ represents the difference in potentials between the solid and solution. The symbol $U_{s,ref}$ denotes the equilibrium potential of the solvent reduction reaction, which we assume to be constant. The total intercalation current J_{tot} represents the flow of charge exchanged with the anode-side solution. Specifically, the total intercalation current J_{tot} is given by the sum of current between the solid and solution (J_1), and the solvent reduction reaction and solution (J_s), that is

$$J_{tot} = J_1 + J_s \quad (6)$$

Equations (2)-(6) encompass the film growth subsystem of the Li-ion battery cell model, adopted from [9]. This subsystem connects to the remainder of the battery model through the total intercalation current J_{tot} and potential difference $\Delta\phi$. Since these variables vary with respect to space (across the electrodes and separator) and time, they are determined by solving coupled partial differential equations and algebraic constraints representing the concentration and potential distributions in the solid and solution of the anode, cathode, and separator (see [7], [8] for details). For the lithium-ion cells studied in this paper the parameters pertaining to SOC dynamics have been fitted using a custom-built battery test rig. Details on the experimental setup and identification procedure can be found in [22]. Although this model accounts for complex electrochemical phenomena such as diffusion dynamics and film growth, its complexity makes control design for health management difficult. Therefore, the present research seeks to use the high fidelity model to generate simpler models for the purposes of control design.

B. Static Approximation of Film Growth Rate

To acquire insight on the relationship between battery cell SOC, current, and film growth rate, consider an ideal fresh
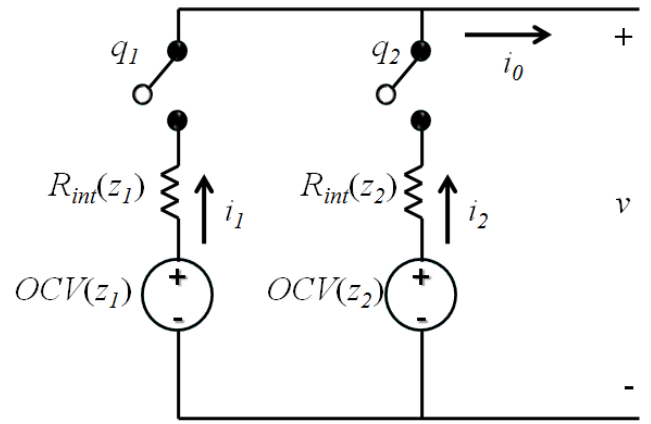
cell, that is $\delta_{film}(x,0) = 0$. Suppose all the intercalation currents, overpotentials, and concentration profiles are constant with respect to space and correspond to zero initial applied current. Starting from these initial conditions, we simulate the electrochemical battery cell model for different initial SOC and applied current levels and measure the instantaneous film growth rate. From these data we produce a static relationship mapping cell SOC and applied current to the spatially averaged film growth rate $\dot{\bar{\delta}}_{film}$, shown in Fig. 2.

The map indicates that film growth rate increases with cell SOC. The film growth rate also increases as the discharge current becomes increasingly negative, i.e. for increasing charge current. Finally, film grows when zero current is applied, indicating that aging occurs even when the cells are not in use. The authors of [9] assume film growth occurs only during charging. However, we simulate the side reaction equations under all applied current conditions and allow the side reaction overpotential to govern film growth. In Section V-E we consider alternative film growth model realizations by (1) obeying the assumption in [9] and (2) using a specific set of alternative model parameter values. A key question we revisit after obtaining the optimal control solution is what insight can be extracted from this map to design controllers that reduce film formation in battery packs?

C. Battery Pack Model

Switched capacitor circuits [5], [6] are typically applied to equalize individual SOC levels for cells connected in series. In this article, we examine the potential advantages of allowing unequal charge levels for battery modules connected in parallel. A simple method to independently control module charge levels uses switches in protection circuits [23] (e.g. solid state relays or contactors). These devices are primarily designed to disconnect the battery in case of imminent catastrophic behavior, such as thermal runaway [24]. When multiple modules are arranged in parallel, individual solid state relays can be connected in series with each parallel branch. These relays may serve as one potential opportunity for individually controlling battery module SOC, and will be the topology we consider henceforth.

Consider a battery pack architecture consisting of two modules connected in parallel through two switches, where each module contains one cell for simplicity (Fig. 3). The goal is to determine the optimal switching strategy that minimizes the total film growth of both cells, given an exogenous current trajectory i_0. Due to the computational complexity of the distributed parameter electrochemical cell model described in Section 2.1, and the curse of dimensionality imposed by dynamic programming [25], we require a simplified model for control design. As such, we utilize an equivalent circuit model [16], [26], written in discrete time, with a ten second time step ($\Delta T = 10$ sec). This equivalent circuit model consists of an open circuit voltage source OCV in series with an internal resistor R_{int}. Open circuit voltage and internal resistance are nonlinear functions of SOC, that is $OCV(z_i)$ and $R_{int}(z_i)$ where $i = 1, 2$. The state variables z_1 and z_2 represent the SOC of battery cells 1 and 2 respectively. The dynamic equations for each cell are based on integrating current i_1, i_2 to obtain charge, and then dividing by the total charge capacity of the cell Q.

$$z_{1,k+1} = z_{1,k} - \frac{i_{1,k}}{Q}\Delta T \tag{7}$$

$$z_{2,k+1} = z_{2,k} - \frac{i_{2,k}}{Q}\Delta T \tag{8}$$

The currents i_1, i_2 are determined by the configuration of the switches and exogenous current demand on the battery pack i_0. The currents are given by Kirchoff's current law, where the switching signals q_1 and q_2 equal zero and one when the corresponding switch is respectively open or closed:

$$i_{1,k} = q_{1,k}(1 - q_{2,k})i_{0,k} \tag{9}$$
$$+ \frac{OCV(z_{1,k}) - OCV(z_{2,k}) + i_{0,k}R_{int}(z_{2,k})}{R_{int}(z_{1,k}) + R_{int}(z_{2,k})}q_{1,k}q_{2,k}$$

$$i_{2,k} = (1 - q_{1,k})q_{2,k}i_{0,k} \tag{10}$$
$$+ \frac{OCV(z_{2,k}) - OCV(z_{1,k}) + i_{0,k}R_{int}(z_{1,k})}{R_{int}(z_{1,k}) + R_{int}(z_{2,k})}q_{1,k}q_{2,k}$$

The first terms on the right-hand sides of (9) and (10) model one cell connected at a time. The second terms model when both cells are connected. When both q_1 and q_2 equal zero neither cell charges (i.e. both cells experience zero current).

The parameters OCV and R_{int} for the equivalent circuit model are identified from experimental characterization of commercial lithium-ion cells with LiFePO$_4$ cathode chemistries. The measured values are provided in Fig. 4. The open circuit voltage is determined by charging and discharging the cells at a C/10 rate across the entire voltage range. Then we average the measured terminal voltage for each SOC value. Internal resistance is determined by applying step changes in current and measuring the associated jump in terminal voltage, for each SOC value. This is done for both charging and discharging, rendering internal resistance as a function of SOC and direction of current flow.

III. OPTIMAL CONTROL PROBLEM FORMULATION

The control objective is to determine the optimal switching sequence that minimizes the total resistive film growth in the
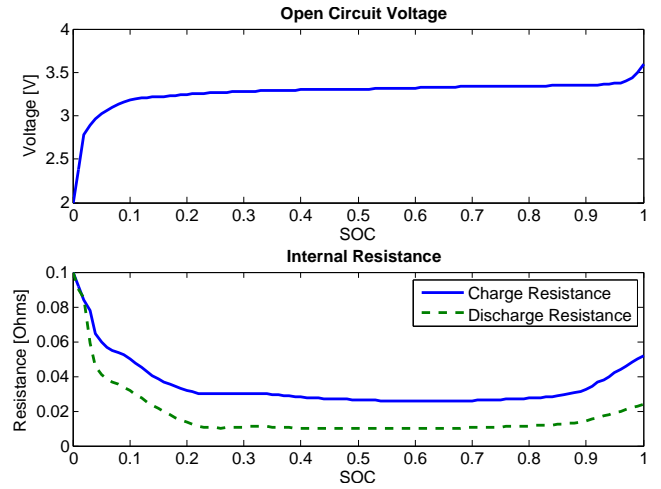

Fig. 4. Parameterization of equivalent circuit battery model identified from commercial lithium-ion cells with LiFePO$_4$ cathode chemistries. [Top] Open circuit voltage and [Bottom] internal resistance.

battery pack described in Section 2, given a current trajectory, i_0, known *a priori*. We formulate this as a finite horizon constrained optimal control problem

$$\min_{(q_1,q_2)} J = \sum_{k=0}^{N}\left[\sum_{j=1}^{2}\dot{\bar{\delta}}_{film}(z_{j,k}, i_{j,k}) + g_z(z_k)\right]$$
$$+ \alpha_N\|z_N - 0.95\|_2^2 \tag{11}$$

subject to

$$z_{k+1} = f(z_k, i_k) \tag{12}$$
$$i_k = h(q_k, i_{0,k}) \tag{13}$$
$$z_0 = z_{ic} \tag{14}$$

where

$$(q_1, q_2) \in \{0, 1\} \times \{0, 1\} \tag{15}$$

$$g_z(z_k) = \alpha_z\left[\sum_{i=1,2}\max\{0.05 - z_{i,k}, 0, z_{i,k} - 0.98\}\right]^2 +$$

$$\alpha_v\left[\sum_{i=1,2}\max\{2.0 - v_{i,k}, 0, v_{i,k} - 3.6\}\right]^2 \tag{16}$$

$$z_k = [z_{1,k}\ z_{2,k}]^T \tag{17}$$
$$i_k = [i_{1,k}\ i_{2,k}]^T \tag{18}$$

where the function $\dot{\bar{\delta}}_{film}$ maps SOC and current to average film growth rate according to the relationship depicted in Fig. 2. The function $g_z(z_k)$ denotes soft constraints that limit cell SOC and cell voltage to protect against over-charging and over-discharging. However, for the simulation described in this article, these constraints never become active due to the modest charging rate employed. A terminal constraint with weighting α_N is provided to ensure the battery pack charges to the SOC corresponding to the desired final voltage. The function $f(z_k, i_k)$ represents the dynamic equation in (7)-(8). The function $h(q_k, i_{0,k})$ maps the switch position and battery
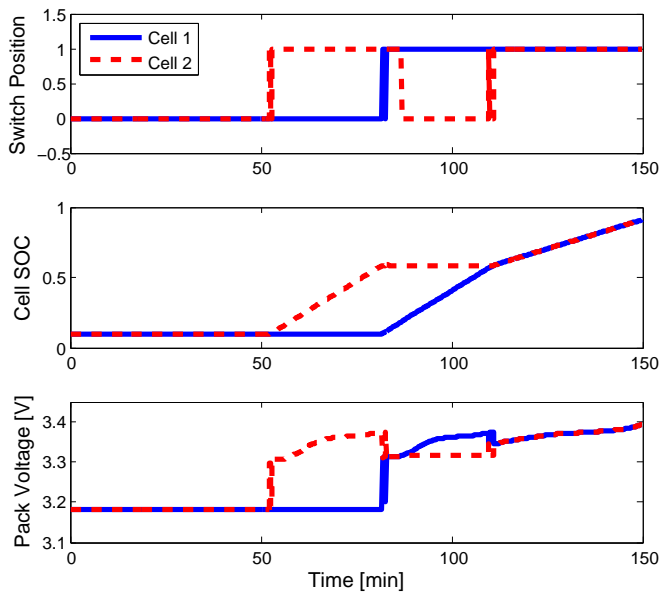
Fig. 5. Time responses for optimal charging pattern identified by DDP, given a 1C battery pack charge rate.

Fig. 6. Optimal trajectories for various initial conditions, given a 1C battery pack charge rate.

pack current to cell current in (9)-(10). Finally, we impose a fixed initial condition z_{ic}.

To solve the optimization problem in (11)-(18), we re-express the equations as a dynamic programming problem by defining a value function as follows [25]: Let $V_k(z_k)$ represent the minimum total film growth from discrete time k to the end of the time horizon, given that the cell SOC in the present time step k is given by the vector z_k. Then the optimization problem can be written as the following recursive Bellman optimality equation and boundary condition.

$$V_k(z_k) = \min_{(q_1,q_2)} \left\{ \begin{array}{l} \sum_{j=1}^{2} \dot{\bar{\delta}}_{film}(z_{j,k}, i_{j,k}) \\ +g_z(z_k) + V_{k+1}(z_{k+1}) \end{array} \right\} \quad (19)$$

$$V_N(z_{N-1}) = \min_{(q_1,q_2)} \left\{ \alpha_N \|z_N - 0.95\|_2^2 \right\} \quad (20)$$

The above dynamic programming problem is solved via a full enumeration algorithm. That is, we compute a family of optimal trajectories for a set of fixed initial conditions. This approach enables us to analyze an ensemble of trajectories to gain insight on how DDP minimizes total film growth.

IV. SOLUTION ANALYSIS

A. Analysis of Optimal Trajectories

To acquire insight on the optimal switching sequence for minimizing resistive film growth, we consider a constant 1C (2.3 A) charge rate applied to the battery pack. Note that while the battery pack experiences a constant current charge rate, the individual cells will have time-varying charge rates. Time responses for an initial SOC of 0.1 for each cell are provided in Fig. 5. Figure 6 demonstrates the optimal trajectories for a set of initial battery cell SOC conditions. These figures indicate that the optimal switching sequence follows a consistent pattern:
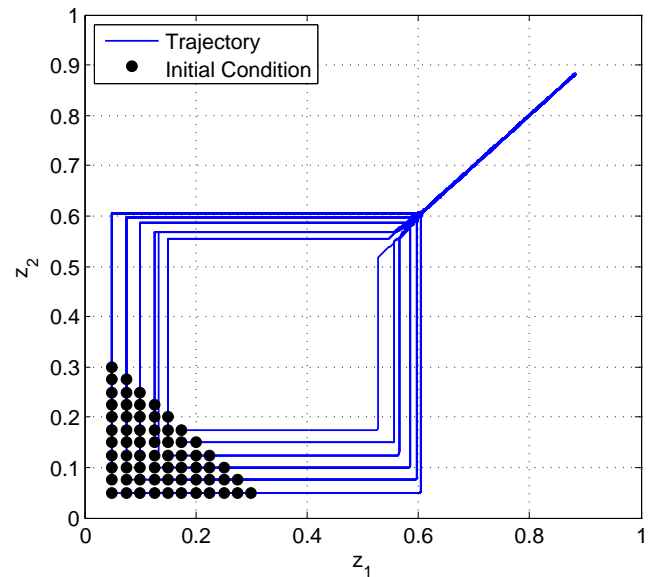
1) Leave the battery pack uncharged for as long as possible. This minimizes the duration of time over which the pack's cells have large SOC values and, consequently, large film buildup rates.
2) Charge the cell with greater initial SOC.
3) Charge the cell with less SOC until both cells approximately equalize.
4) Charge both cells together, at approximately equal current values, until the final state is reached.

The key question is why does DDP identify the pattern in Steps 2-4 above as the optimal switching sequence for minimizing film growth?

B. The Energy Storage-Film Growth Tradeoff

First, consider the result that film growth is minimized by leaving the battery pack uncharged for as long as possible. This is, film growth is minimized if battery packs are charged only immediately before use. This result was also found in a recent study on charge trajectory optimization for plug-in hybrid electric vehicles [22]. The reason for this result can be seen by observing that the film growth rate increases with SOC in Fig. 2. Therefore, maintaining each cell in a low SOC reduces the overall film buildup. However, this requires *a priori* knowledge of when the battery pack will be used. Moreover, if the battery is discharged sooner than expected, only a fraction of the total energy capacity is available for use. This suggests a fundamental tradeoff between electric energy storage and reducing anode-side film growth.

C. Convexity Analysis of Film Growth Rate

To answer the fundamental question of why DDP identifies the particular charging pattern described above, let us focus on the switching pattern exhibited by the optimal solution when charging does occur. Consider the film growth rate for varying
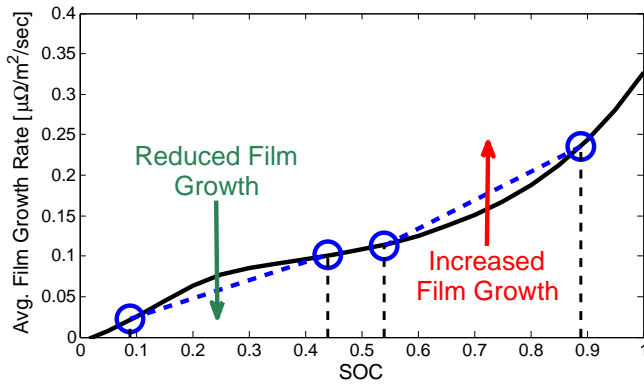
Fig. 7. Convexity analysis of spatially-averaged film growth rate for zero applied current.

SOC and zero current input, as portrayed in Fig. 7. For small SOC values, $\dot{\bar{\delta}}_{film}$ is concave. Along this portion of the curve, the total film growth rate for two cells at different SOC values is less than the total film growth rate for two cells at the same SOC value. However, for large SOC values $\dot{\bar{\delta}}_{film}$ is convex. This implies that the total film growth rate for two cells at different SOC values is greater than the total film growth rate for two cells at equal SOC values. If one assumes the solution is infinitely greedy, these observations for reducing film growth can be applied as follows:

1) In the concave region of $\dot{\bar{\delta}}_{film}$, drive the individual SOC values apart.
2) In the convex region of $\dot{\bar{\delta}}_{film}$, equalize the individual SOC values.

In other words, charge each module one-by-one through the concave region and then charge them all simultaneously.

These results indicate that a reduction in total film growth can be achieved by allowing individual modules to have unequal SOC values - particularly within concave regions of film growth. This result motivates the health reduction opportunities for battery management systems if certain convexity properties can be identified for lithium battery degradation mechanisms. Additionally, the optimal policy follows a consistent pattern that may be closely approximated by a heuristic feedback control law, which leaves the battery discharged for the maximum allowable time.

D. DDP-inspired Heuristic Control

Inspired by these results, and the convexity analysis presented in Section IV-C, we examine a heuristic control scheme for minimizing film growth, depicted in Fig. 8. The advantage of a heuristic control scheme over the optimal trajectories computed by DDP is that the former can be implemented in a feedback loop. Additionally, one expects the heuristic scheme to achieve nearly optimal performance, due to the consistent pattern exhibited by the DDP solutions. The process of converting optimal trajectories into an explicit feedback map has been studied in model predictive control theory [27]. These concepts are potentially applicable here, but a simpler less formal approach is used in this initial study. Note that
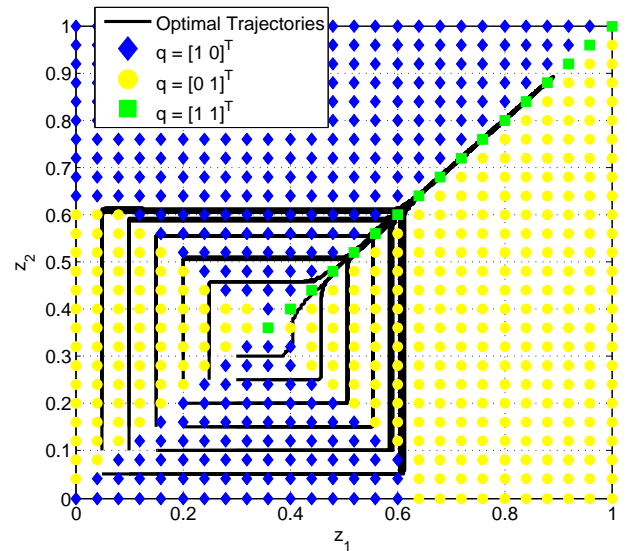

Fig. 8. DDP-inspired heuristic rule for charging, with optimal state trajectories superimposed.

the switching pattern defined by the heuristic rule should not be initiated until the last possible opportunity. In this example, each cell has a 1.8 A-h charge capacity and thus the total pack charge capacity is 3.6 A-h. Therefore charging both cells from 0.1 SOC to 0.95 SOC at a 1C (1.8 A) rate requires about 100 minutes. As a result, we initiate the heuristic charging scheme 100 minutes prior to the final time.

The design of the heuristic control law follows two steps: First, we simulate the optimal trajectories from a family of initial conditions, such as shown in Fig. 6. Second, we identify regions of the state-space corresponding to a certain switch configuration. For regions in which the optimal state trajectories do not enter, we select a switch configuration that steers the state toward an optimal trajectory. This step is required, because for the 1C charge rate input studied here, feasible trajectories do not cover the entire state-space. The final result of this procedure is depicted in Fig. 8, where several optimal state trajectories are superimposed on the proposed heuristic rule. Note how the heuristic controller follows the general guidelines of SOC separation and equalization in the respective concave and convex regions of Fig. 7.

V. COMPARATIVE ANALYSIS AND SENSITIVITY STUDIES

To evaluate the performance of the proposed heuristic controller, we compare it to the optimal DDP-based and standard equalization schemes (i.e. both switches closed during charging). We perform this study by simulating the closed loop battery pack degradation control system for a 1C (2.3 A) constant current charge rate cycle. This study is performed on both the equivalent circuit model and static map of film growth rate (which was used for optimization, and henceforth is referred to as the "Control" model) and the full electrochemical model. In both cases the initial cell SOC values are 0.1 each. In practice, the standard charge method is to apply constant current to every cell in the pack until the voltage
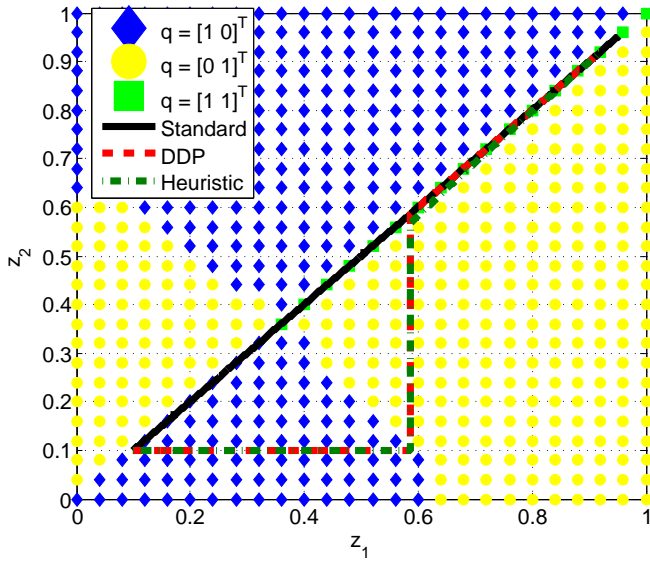
Fig. 9. SOC trajectories for each control scheme, superimposed on the heuristic control map.
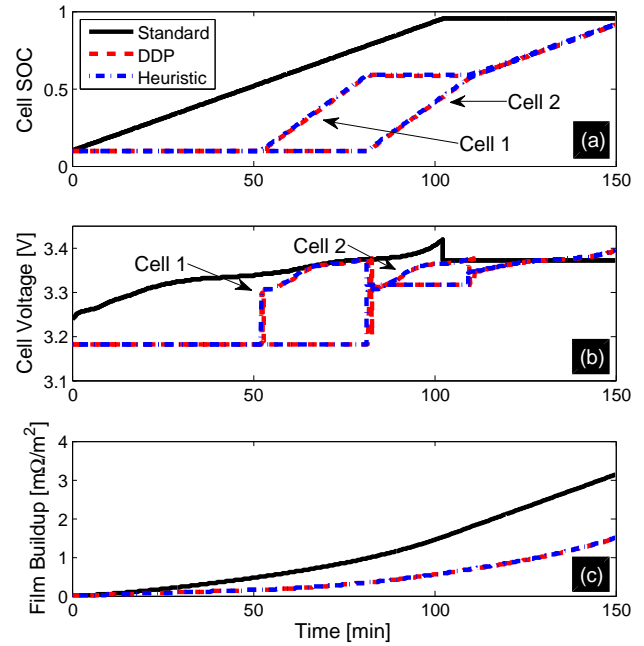

Fig. 10. Time responses for each control scheme.
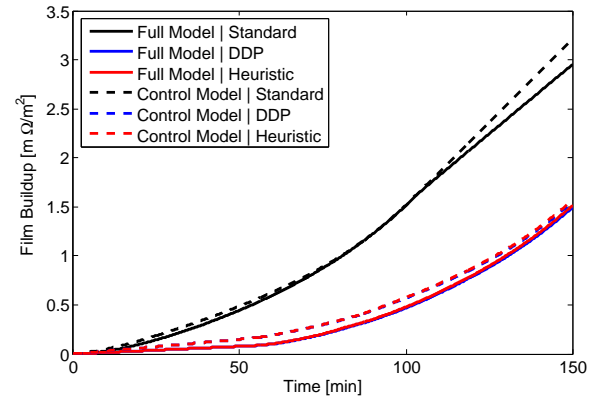

Fig. 11. Film Buildup for each control scheme, simulated on the control model and full electrochemical model.

reaches a maximum value, then the voltage is held constant at this maximum value until the applied current reaches some minimal level. This is known as a constant current, constant voltage (CCCV) charge cycle [9]. Here, we only investigate the potential improvements incurred during the period when the cells charge up to a maximum voltage limit, corresponding to 0.95 SOC in our simulations. Subsequently, we report on similar results obtained for constant current *discharge* inputs. Finally, we analyze optimal switch patterns for alternative film growth maps, created using different assumption sets or model parameters. The latter analysis is motivated by the fact that accurately modeling aging in lithium batteries is extremely difficult - due to the extensive array of degradation mechanisms and materials within lithium-ion batteries. Regardless of these differences, the link between convexity properties and unbalanced cells remains in our studies.

A. Control Model Charge Cycle Simulation

The cell SOC trajectories for each control scheme simulated on the Control model are provided in Fig. 9, superimposed on the heuristic rule. Observe that the standard charging scheme maintains each cell at equal SOC values as the battery pack charges. In contrast, the trajectories corresponding to DDP and the heuristic rule follow trajectories similar to Fig. 6 and 8. Namely, both methods charge one cell at a time in the concave region of $\bar{\dot{\delta}}_{film}$, and then apply charge equalization in the convex region of $\bar{\dot{\delta}}_{film}$. Also observe that trajectories for DDP and the heuristic controller match closely, indicating that the proposed heuristic controller closely approximates the optimal solution for the trajectory shown here.

Time responses for the cell SOC, current, and battery pack voltage are provided in Fig. 10. Here we see that the heuristic rule is initiated approximately 50 minutes into the simulation, allowing 100 minutes of charging time. Figure 10(a)-(c)

further demonstrate how closely the heuristic controller and DDP solution match, with respect to time. Since the standard method initiates charging immediately, the cells remain idle at 0.95 SOC once charging is complete. This is important because film builds up at a faster rate for high SOC relative to low SOC, which is the intuitive reason why delayed charging significantly reduces total film buildup. The impact of this property can be seen in Fig. 10(c). Figure 10(b) demonstrates each cell's voltage, which increases only when that particular cell is charging. Note that all schemes maintain the cell voltage within the safety range of 2.0V to 3.6V.

B. Film Buildup Validation on Full Electrochemical Model

To this point, all simulation results have been performed on a reduced equivalent circuit model and static film growth rate map in Fig. 2 used for control optimization. In this subsection

we study (1) if optimal switching indeed reduces film buildup for a high-fidelity electrochemical battery model, and (2) if the static approximation of film growth reasonably matches the film model prediction. Towards this goal, we apply all three controllers (standard, DDP, and heuristic) on the full electrochemical model (Full).

The aggregated film buildup for the Control and Full models, simulated using each control scheme, are provided in Fig. 11. This figure indicates that the DDP and heuristic control schemes indeed reduce film buildup on the full electrochemical model, despite being synthesized for the Control model. Specifically, the open-loop DDP control and closed-loop heuristic controller reduced buildup by 49.5% and 48.7%, respectively. Moreover, the total film growth predicted by the Control model differ from the Full model by less than 10% for all control schemes. Therefore, we conclude that the reduced order model, taking the form of a static nonlinear map, enables the accurate minimization of film growth for the charge cycles studied here.

C. Performance Results

A comparison of the performance for each control scheme is provided in Table I. For the 2.3A rate charge cycle studied in this article, the heuristic controller produces an additional 20 $\mu\Omega/m^2$ (0.8%) of resistive film buildup over the DDP solution on the full electrochemical model. Hence, the heuristic scheme exhibits nearly identical performance to the optimal control design. Both DDP and the heuristic controller reduce film buildup by about 50%, for this charge cycle. It is important to note that the reduction in film buildup is a function of the particular charge cycle and time horizon. That is, cycles that remain within the concave region of $\bar{\delta}_{film}$ may experience greater improvement, because the switched scheme proposed in this article has the greatest advantage in this domain. Moreover, the bulk of film reduction occurs due to delaying the charging process to the end of the time horizon. For the example studied here, 48% of film buildup reduction is due to delaying charging until the final 100 minutes.

D. Optimal Trajectories for Discharge

Throughout this article, we have consider optimally connecting battery cells in parallel with relay switches to minimize total film growth - under charging events only. Here we consider constant current *discharge* events. The problem is formulated exactly as before, except now we apply a 2.3A discharge current input. The optimal switch, SOC, and voltage trajectories are provided in Fig. 12, with the battery pack initialized at 95% SOC for each cell. Optimal SOC trajectories for various initial conditions are provided in Fig. 13. Under a discharging scenario, these results indicate the optimal constant current discharging trajectories follow a consistent pattern.

1) Discharge the pack immediately. This moves the system away from regions of fast film growth - so less interfacial film accumulates over time.
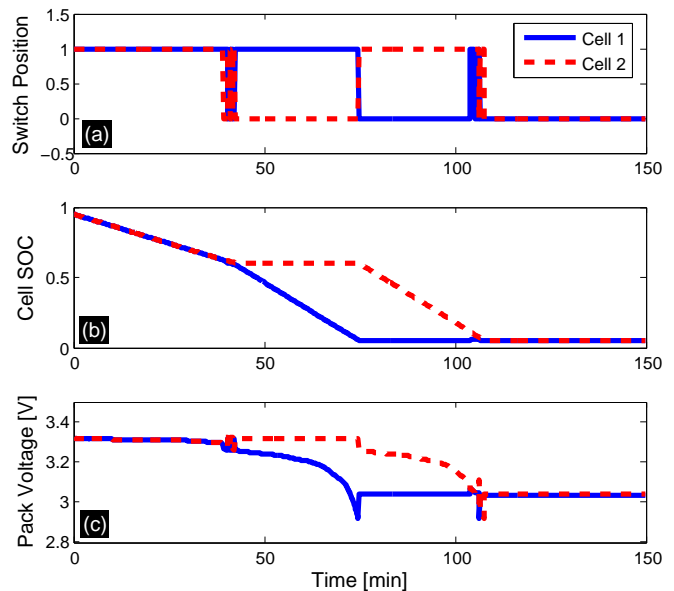2) Equalize both cells as they discharge.

Fig. 12. Time responses for optimal discharging pattern identified by DDP, given a 1C battery pack discharge rate.

3) Continue to discharge both cells at equal charge levels, until a certain point.
4) Discharge each cell individually until the battery pack is fully discharged.

In essence, these discharge trajectories follow the optimal charge trajectories backwards. Moreover, the breakpoint between charge equalization and unequalization is approximately the same - 60% for both cells. Convexity arguments for infinitely greedy trajectory optimization solutions can be applied, once again, to interpret these results. Hence, allowing unequal charge levels in battery management systems may provide long-term health benefits when concavity properties exist in the aging mechanics.

E. Sensitivity to Alternative Film Growth Parameterizations

Anode-side film growth has been recognized as a significant contributor to lithium-ion battery health degradation [12]. However a plethora of other difficult-to-model aging mechanisms can contribute to capacity and power fade. Moreover, modeling and accurately parameterizing these models across a wide range of lithium-ion cell chemistries and manufacturers can be difficult. This motivates the sensitivity analysis presented here. Specifically, we consider alternative film growth maps to evaluate the generality of unbalanced charging to varying model assumptions and parameterizations.

TABLE I
CONTROLLER PERFORMANCE COMPARISON ON CONTROL MODEL AND FULL ELECTROCHEMICAL MODEL.

| Control Scheme | Control Model | | Full Model | | |
	Resistance of Total Film Buildup	Reduction in Film Buildup	Resistance of Total Film Buildup	Reduction in Film Buildup	Control vs. Full Error
Standard	3.20 mΩ/m^2	0%	2.95 mΩ/m^2	0%	8.47%
DDP	1.55 mΩ/m^2	51.8%	1.49 mΩ/m^2	49.5%	4.03%
Heuristic	1.56 mΩ/m^2	51.2%	1.51 mΩ/m^2	48.7%	3.31%
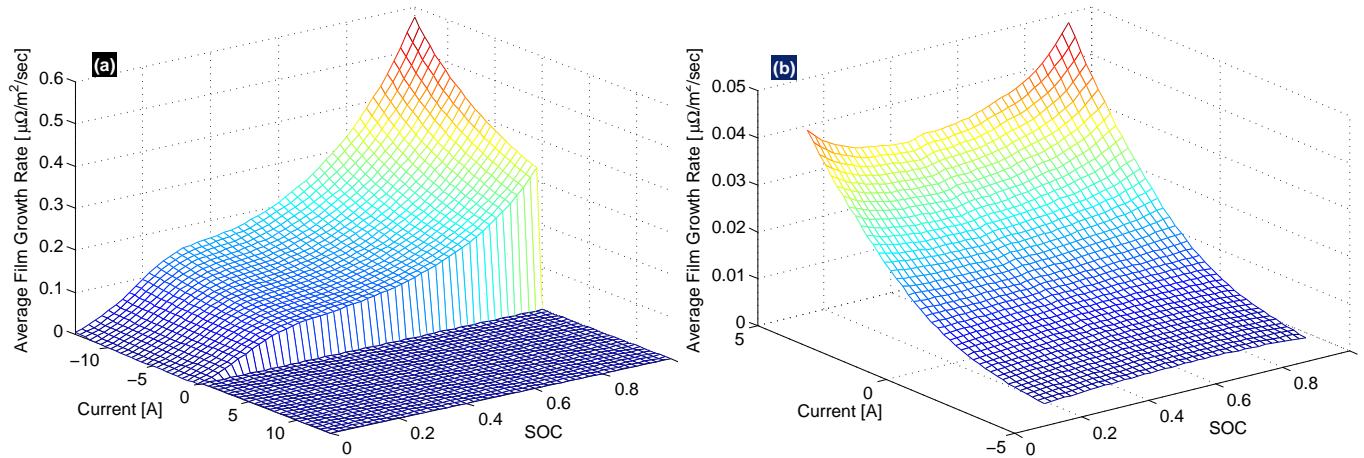
Fig. 14. Film growth maps for alternative electrochemical model parameterizations: (a) No film growth occurs during discharge or rest conditions, which follows Assumption 2 of [9]; (b) Preliminary parameterization to match the manufacturer's cycling and storage performance data.

Fig. 15. Time responses of optimal charging trajectories for the alternative film growth maps. (a) Response for map in Fig. 14(a). This map suggests charging the battery pack one cell at a time. (b) Response for map in Fig. 14(b). This map suggests charge equalization is optimal.

Fig. 13. Optimal trajectories for various initial conditions, given a 1C battery pack discharge rate.
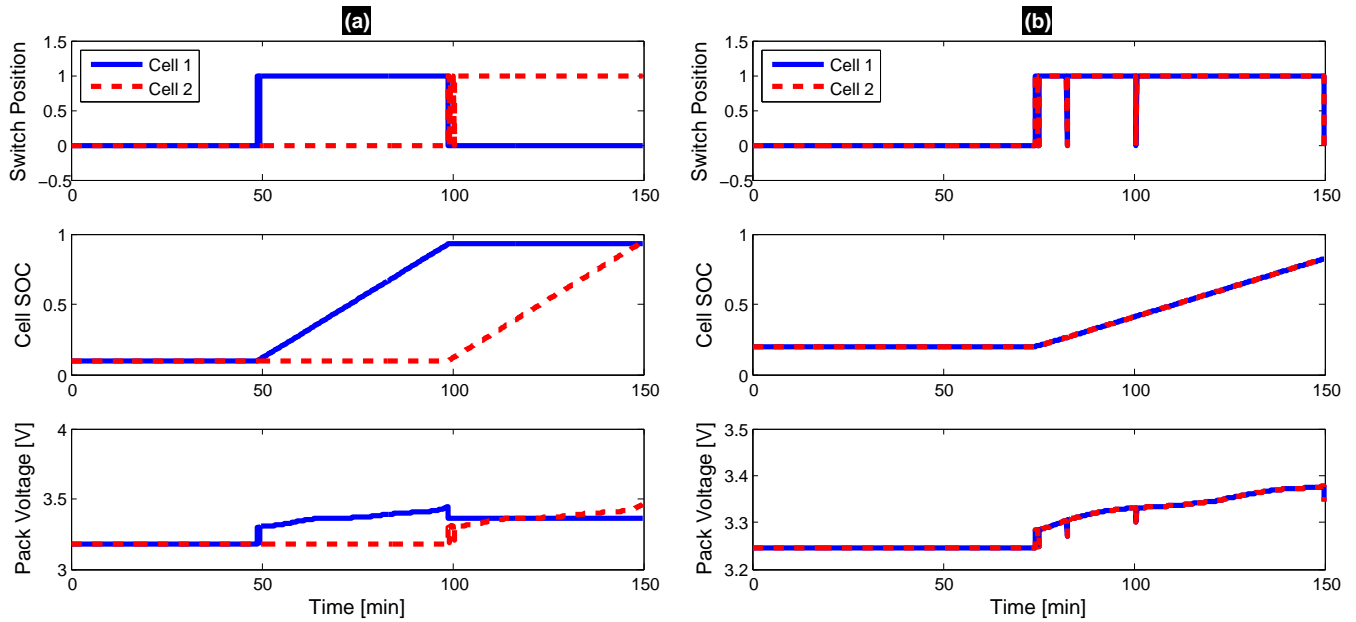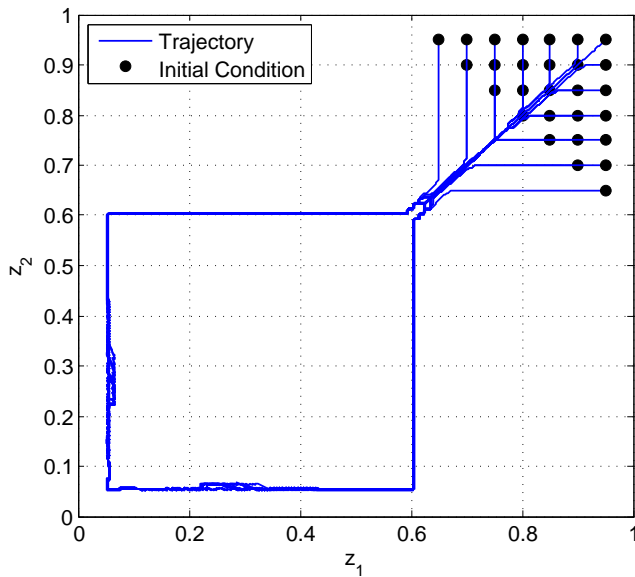
The first map, shown in Fig. 14(a), is equivalent to Fig. 2 except we enforce Assumption 2 of [9] which states that film growth occurs only during charging events, i.e. zero growth during rest and discharge conditions. The optimal charge trajectories for a 1C constant current rate are shown in Fig. 15(a). In this case the optimal solution charges each cell individually and in succession. This result can be understood by noting that one cell charged at 1C and the other at rest (no growth) produces less total film growth than two cells charged simultaneously at 0.5C. Also note that although Fig. 15(a) shows a delayed charging strategy, delaying charging provides equivalent film growth as immediate charging since zero film growth occurs during rest. Therefore when Assumption 2 of [9] holds true, unbalanced charging provides a 53% reduction in total film growth, which is a greater reduction from unbalanced charging when using the original film growth map.

The second map, shown in Fig. 14(b), is based upon the same model equations used for Fig. 2 but with an alternative parameter set. This parameter set has been identified to produce capacity fade trends that match the manufacturer's cycling and storage data [22]. The two parameter sets used for each map are provided in Appendix B. The optimal charge trajectories for a 1C constant current rate are shown in Fig. 15(b). Unlike the previous two cases the optimal solution does not unbalance the cells' charge levels. This result can be interpreted through the convexity arguments of Section IV-C by observing that Fig. 15(b) contains no concave regions. Thus charge balancing minimizes film growth. However, delayed charging still provides benefits by maximizing the time spent to low SOC levels, where film growth is slow.

VI. CONCLUSIONS

This research investigates battery health management in lithium ion battery packs using relay switches for modules

connected in parallel. To facilitate control design and analysis, we consider an electrochemical battery cell model with irreversible solvent reduction reaction dynamics at the anode, developed by Ramadass *et. al.* [9]. From this high fidelity model, we approximate film growth rate as a static map that functionally depends on cell SOC and applied current. Using this map, we formulate an optimal control problem to minimize total battery pack film growth for a constant current charge trajectory. Inspired by the optimal trajectories, and the convexity properties of the film growth map, we design a heuristic rule base that produces nearly optimal performance. Further optimization results for constant current discharge trajectories and alternative film growth models demonstrate the generality of charge unequalization to varying input profiles, model assumptions, and parameterizations.

The key result demonstrated by this work is that health degradation due to film growth can be reduced by: (1) Allowing battery modules connected in parallel to attain unequal SOC values when concavity features exist; and (2) Delaying charging until immediately before discharging. Indeed, the optimal solution approximately separates SOC in the concave region and equalizes SOC in the convex region of film growth rate at the end of the time horizon. This process can be implemented using a heuristic static feedback controller designed from optimal trajectories computed via dynamic programming. Individual control of module SOC is achieved via relay switches typically used for safety precautions. Within each module, individual cell SOC may be equalized via traditional switched capacitor circuits [5], [6] to protect against over-charging or over-discharging. Simulation results indicate this approach may significantly reduce total battery pack film growth, if one can identify concavity features in the degradation performance map. This motivates future work focused in two directions. First, experimentally identifying a data-driven degradation map similar to Fig. 2 may enable significant improvements in lithium ion battery lifetime through charge unbalancing schemes. Second, experimental verification of these algorithms designed from data-driven degradation models will provide the ultimate proof-of-concept.

APPENDIX A
NOMENCLATURE

Symbol	Description	Units
F	Faraday's constant	[C/mol]
i_0	Battery pack current	[A]
$i_{0,s}$	Exchange current density for side reaction	[A/m^2]
i_1, i_2	Cell current	[A]
$h_{penalty}$	Quadratic penalty function	[pm/m^2]
J	Cost functional	[pm/m^2]
J_1	Intercalation current between solid and solution	[A/m^3]
J_p	Terminal state penalty function	[pm/m^2]
J_{tot}	Total intercalation current	[A/m^3]
J_s	Side rxn. current density	[A/m^3]

This article has been accepted for publication in a future issue of this journal, but has not been fully edited. Content may change prior to final publication.

IEEE TRANSACTIONS ON INDUSTRIAL ELECTRONICS 11

Symbol	Description	Units
M_P	Molecular weight of product from side reaction	[mol/kg]
Q	Battery cell charge capacity	[A·h]
q_1, q_2	Contactor switch position	
R	Universal gas constant	[J/K/mol]
R_{film}	Total film resistance at electrode/electrolyte interface	[Ω·m^2]
R_{int}	Battery cell internal resistance	[Ω]
R_{SEI}	Resistance of solid electrolyte interphase (SEI)	[Ω/m^2]
$U_{s,ref}$	Equilibrium potential of side reaction	[V]
V	Value function	[pm/m^2]
v	Battery pack voltage	[V]
x	Spatial coordinate	[m/m]
z	Battery cell state of charge	[C/C]
$\Delta\phi$	Local potential difference b/w solid and solution at anode	[V]
δ_{film}	Resistive film thickness	[pm/m^2]
η_s	Overpotential driving side rxn.	[V]
κ_P	Side rxn. product conductivity	[1/m/Ω]
ρ_P	Side rxn. product density	[kg/m^2]

APPENDIX B

FILM GROWTH MODEL PARAMETERS

	Values for map depicted in	
Symbol	Fig. 2 & 14(a)	Fig. 15(b)
$i_{0,s}$	1.5×10^{-6} A/m^2	4×10^{-8} A/m^2
M_P	73000 mol/kg	73000 mol/kg
R_{SEI}	7.4 mΩ·m^2	7.4 mΩ·m^2
$U_{s,ref}$	0.4 V	0.4 V
κ_P	1 (m·Ω)$^{-1}$	1 (m·Ω)$^{-1}$
ρ_P	2100 kg/m^2	2100 kg/m^2
$U_{ref,n}(\theta_n)$	Adopted from [9]	Adopted from [22]

REFERENCES

[1] B. K. Sovacool and R. F. Hirsh, "Beyond batteries: An examination of the benefits and barriers to plug-in hybrid electric vehicles (PHEVs) and a vehicle-to-grid (V2G) transition," *Energy Policy*, vol. 37, no. 3, pp. 1095–1103, 3 2009.

[2] M. Alamgir and A. M. Sastry, "Efficient batteries for transportation applications," *SAE Paper 2008-21-0017*, 2008.

[3] J. Chatzakis, K. Kalaitzakis, N. Voulgaris, and S. Manias, "Designing a new generalized battery management system," *IEEE Transactions on Industrial Electronics*, vol. 50, no. 5, pp. 990–999, Oct. 2003.

[4] Y.-S. Lee and M.-W. Cheng, "Intelligent control battery equalization for series connected lithium-ion battery strings," *IEEE Transactions on Industrial Electronics*, vol. 52, no. 5, pp. 1297–1307, Oct. 2005.

[5] J. W. Kimball, B. T. Kuhn, and P. T. Krein, "Increased performance of battery packs by active equalization," *2007 IEEE Vehicle Power and Propulsion Conference*, Sept. 9-12 2007 2007.

[6] A. Baughman and M. Ferdowsi, "Double-tiered switched-capacitor battery charge equalization technique," *IEEE Trans. on Industrial Electronics*, vol. 55, no. 6, pp. 2277–85, 2008.

[7] M. Doyle, T. Fuller, and J. Newman, "Modeling of galvanostatic charge and discharge of the lithium/polymer/insertion cell," *Journal of the Electrochemical Society*, vol. 140, no. 6, pp. 1526 – 33, 1993.

[8] T. Fuller, M. Doyle, and J. Newman, "Simulation and optimization of the dual lithium ion insertion cell," *Journal of the Electrochemical Society*, vol. 141, no. 1, pp. 1 – 10, 1994.

[9] P. Ramadass, B. Haran, P. Gomadam, R. White, and B. Popov, "Development of first principles capacity fade model for Li-ion cells," *Journal of the Electrochemical Society*, vol. 151, no. 2, pp. 196 – 203, 2004.

[10] L. Kanevskii and V. Dubasova, "Degradation of lithium-ion batteries and how to fight it: A review," *Russian Journal of Electrochemistry*, vol. 41, no. 1, pp. 3 – 19, 2005.

[11] P. Arora, R. E. White, and M. Doyle, "Capacity fade mechanisms and side reactions in lithium-ion batteries," *Journal of the Electrochemical Society*, vol. 145, no. 10, pp. 3647 – 3667, 1998.

[12] D. Aurbach, "Review of selected electrode-solution interactions which determine the performance of Li and Li ion batteries," *Journal of Power Sources*, vol. 89, no. 2, pp. 206 – 18, 2000.

[13] E. Gatzke, A. Stamps, C. Holland, and R. White, "Analysis of capacity fade in a lithium ion battery," *Journal of Power Sources*, vol. 150, pp. 229–39, 10/04 2005.

[14] M. Verbrugge and E. Tate, "Adaptive state of charge algorithm for nickel metal hydride batteries including hysteresis phenomena," *Journal of Power Sources*, vol. 126, no. 1-2, pp. 236–249, 2004.

[15] G. L. Plett, "Extended Kalman filtering for battery management systems of LiPB-based HEV battery packs. Part 1. Background," *Journal of Power Sources*, vol. 134, no. 2, pp. 252–61, 08/12 2004.

[16] G. Plett, "Extended Kalman filtering for battery management systems of LiPB-based HEV battery packs. Part 2. Modeling and identification," *Journal of Power Sources*, vol. 134, no. 2, pp. 262 – 76, 2004.

[17] G. L. Plett, "Extended Kalman filtering for battery management systems of LiPB-based HEV battery packs. Part 3. State and parameter estimation," *Journal of Power Sources*, vol. 134, no. 2, pp. 277–92, 08/12 2004.

[18] K. Smith, C. Rahn, and C.-Y. Wang, "Model-based electrochemical estimation of lithium-ion batteries," *2008 IEEE International Conference on Control Applications (CCA) part of the IEEE Multi-Conference on Systems and Control*, pp. 714 – 19, 2008.

[19] D. Di Domenico, G. Fiengo, and A. Stefanopoulou, "Lithium-ion battery state of charge estimation with a kalman filter based on a electrochemical model," *2008 IEEE International Conference on Control Applications (CCA) part of the IEEE Multi-Conference on Systems and Control*, pp. 702 – 707, 2008.

[20] S. J. Moura, J. L. Stein, and H. K. Fathy, "Control of film growth in lithium ion battery packs via switches," *ASME Dynamic Systems and Control Conference*, Oct. 2009.

[21] J. Newman, *Electrochemical Systems*, 2nd ed. Prentice Hall, 1991.

[22] S. Bashash, S. J. Moura, J. C. Forman, and H. K. Fathy, "Plug-in Hybrid Electric Vehicle Charge Pattern Optimization for Energy Cost and Battery Longevity," *Journal of Power Sources*, vol. 196, no. 1, pp. 541–549, 2011.

[23] P. Balakrishnan, R. Ramesh, and T. Prem Kumar, "Safety mechanisms in lithium-ion batteries," *Journal of Power Sources*, vol. 155, no. 2, pp. 401–414, 2006.

[24] G.-H. Kim, A. Pesaran, and R. Spotnitz, "A three-dimensional thermal abuse model for lithium-ion cells," *Journal of Power Sources*, vol. 170, no. 2, pp. 476 – 89, 2007.

[25] E. Denardo, *Dynamic Programming: Models and Applications*. Courier Dover Publications, 2003.

[26] S. J. Moura, H. K. Fathy, D. S. Callaway, and J. L. Stein, "A stochastic optimal control approach for power management in plug-in hybrid electric vehicles," *ASME Dynamic Systems and Control Conference*, Oct. 2008.

[27] A. Bemporad, F. Borrelli, and M. Morari, "Model predictive control based on linear programming - the explicit solution," *IEEE Transactions on Automatic Control*, vol. 47, no. 12, pp. 1974 – 1985, 2002.

Scott J. Moura (S'09) received the B.S. degree from the University of California, Berkeley, in 2006 and the M.S. degree from the University of Michigan, Ann Arbor, in 2008, both in mechanical engineering, where he is currently pursuing the Ph.D. degree.

His research interests include optimal control, energy conversion systems, and batteries.

Mr. Moura is a recipient of the National Science Foundation Graduate Research Fellowship, University of Michigan Rackham Merit Fellowship, and College of Engineering Distinguished Leadership Award. He has also been nominated for the Best Student Paper Award at the 2009 ASME Dynamic Systems and Control Conference.

Joel C. Forman has received B.S. degrees in both Mechanical Engineering and Applied Mathematics from the Rochester Institute of Technology (2007)and an M.S. degree in Mechanical Engineering from the University of Michigan, Ann Arbor in (2010) where he is currently pursuing a Ph.D. degree. His research interests include model reduction, parameter identification, and batteries.

Saeid Bashash (M'09) is currently a postdoctoral research fellow at the University of Michigan, Ann Arbor. He received his B.Sc. degree from Sharif University of Technology, Tehran, in 2004, and M.Sc. and Ph.D. degrees from Clemson University, South Carolina, in 2005 and 2008, respectively, all in Mechanical Engineering.

His Ph.D. research focused on the modeling and control of piezoactive micro and nano systems, such as piezoelectric actuators and scanning probe microscopy systems. He is currently working on electrochemical battery systems modeling and simulation, vehicle-to-grid integration, and demand-side energy management. His main research interests include modeling, optimization, and control of complex dynamical systems.

Jeff L. Stein is a Full Professor with the Department of Mechanical Engineering, The University of Michigan, Ann Arbor, and is the former Chair of the Dynamic Systems and Control Division of ASME. His discipline expertise is in the use of computer based modeling and simulation tools for system design and control. He has particular interest in algorithms for automating the development of proper dynamic mathematical models (minimum yet sufficient complexity models with physical parameters). His application expertise is the areas of automotive engineering including green energy transportation, machine tool design and lower leg prosthetics. In the area of green transportation he is working to develop the techniques for the design and control of plug-in hybrid vehicles and smart grid technologies that creates a more efficient use of energy, particular that generated from renewable resources, for a lower carbon and other emissions footprint. He has authored or coauthored over 150 articles in journals and conference proceedings.

Hosam K. Fathy received his B.Sc. (Summa cum Laude), M.S., and Ph.D. degrees - all in Mechanical Engineering - from the American University in Cairo, Egypt (1997), Kansas State University (1999), and The University of Michigan, Ann Arbor (2003), respectively.

He has worked as a Control Systems Engineer at Emmeskay, Inc. (2003-2004), a postdoctoral Research Fellow at The University of Michigan (2004-2006), and an Assistant Research Scientist at The University of Michigan (2006-2010), where he won the 2009 Michigan College of Engineering Outstanding Research Scientist Award. He is now an Assistant Professor in the Mechanical and Nuclear Engineering Department at the Pennsylvania State University. He is the founder and director of the Control Optimization Laboratory, which currently employs graduate students and postdocs at both Michigan and Penn State. His research interests including optimal control and model reduction theories and their application to hybrid vehicles, the smart grid, battery modeling and control, and networked hardware-in-the-loop simulation.